



HAL
open science

SHANK3 mutations identified in autism lead to modification of dendritic spine morphology via an actin-dependent mechanism

Nathalie Sans, Christelle M Durand, Julie Perroy, Francois Loll, David Perrais, Laurent Fagni, Thomas Bourgeron, Mireille Montcouquiol

► To cite this version:

Nathalie Sans, Christelle M Durand, Julie Perroy, Francois Loll, David Perrais, et al.. SHANK3 mutations identified in autism lead to modification of dendritic spine morphology via an actin-dependent mechanism. *Molecular Psychiatry*, 2011, 10.1038/mp.2011.57 . hal-00644264

HAL Id: hal-00644264

<https://hal.science/hal-00644264>

Submitted on 24 Nov 2011

HAL is a multi-disciplinary open access archive for the deposit and dissemination of scientific research documents, whether they are published or not. The documents may come from teaching and research institutions in France or abroad, or from public or private research centers.

L'archive ouverte pluridisciplinaire **HAL**, est destinée au dépôt et à la diffusion de documents scientifiques de niveau recherche, publiés ou non, émanant des établissements d'enseignement et de recherche français ou étrangers, des laboratoires publics ou privés.

***SHANK3* mutations identified in autism lead to modification of dendritic
spine morphology via an actin-dependent mechanism**

Abbreviated title: "*SHANK3* mutations in autism and spine morphology"

Christelle M. Durand^{1,3}, Julie Perroy⁴, François Loll^{1,3}, David Perrais⁵, Laurent Fagni⁴,
Thomas Bourgeron^{6,7*}, Mireille Montcouquiol^{2,3*} and Nathalie Sans^{1,3,8}

¹ Molecular and Cellular Neurobiology Group and ² Developmental Neurosciences Group, INSERM, Neurocentre Magendie, Laboratory of "Pathophysiology of Neural Plasticity," U862, 33077 Bordeaux, France; ³ University of Bordeaux, 33077 Bordeaux Cedex, France;

⁴ Institute of Functional Genomics, CNRS UMR5203, INSERM U661, University of Montpellier I and II, Montpellier, France;

⁵ Laboratoire Physiologie Cellulaire de la Synapse, CNRS UMR 5091, University of Bordeaux, 33077 Bordeaux, France ; ⁶ Human Genetics and Cognitive Functions, Pasteur Institute, Paris, France;

⁷ University Denis Diderot Paris 7, Paris, France

⁸ Correspondence should be addressed to Nathalie Sans, *U862, Neurocentre Magendie, Bordeaux*,
E-mail: nathalie.sans@inserm.fr

* *Equal contribution*

Abstract

Genetic mutations of *SHANK3* have been reported in patients with intellectual disability, autism spectrum disorder (ASD) and schizophrenia. At the synapse, **Shank3/ProSAP2** is a scaffolding protein that connects glutamate receptors to the actin cytoskeleton via a chain of intermediary elements. While genetic studies have repeatedly confirmed the association of *SHANK3* mutations with susceptibility to psychiatric disorders, very little is known about the neuronal consequences of these mutations. Here, we report the functional effects of two *de novo* mutations (STOP and Q321R) and two inherited variations (R12C and R300C) identified in patients with ASD. We show that Shank3 is located at the tip of actin filaments and enhances its polymerization. Shank3 also participates in growth cone motility in developing neurons. The truncating mutation (STOP) strongly affects the development and morphology of dendritic spines, reduces synaptic transmission in mature neurons, and also inhibits the effect of Shank3 on growth cone motility. The *de novo* mutation in the ankyrin domain (Q321R) modifies the roles of Shank3 in spine induction and morphology and actin accumulation in spines and affects growth cone motility. Finally, the two inherited mutations (R12C and R300C) have intermediate effects on spine density and synaptic transmission. Therefore, although inherited by healthy parents, the functional effects of these mutations strongly suggest that they could represent risk factors for ASD. Altogether, these data provide new insights into the synaptic alterations caused by *SHANK3* mutations in humans and provide a robust cellular readout for the development of knowledge-based therapies.

Keywords: Shank3, autism, hippocampus, spine, actin, axonal outgrowth.

Introduction

Autism spectrum disorders (ASD) are heterogeneous neurodevelopmental disorders diagnosed on the basis of three behaviorally altered domains: social deficits, impaired language and communication, and stereotyped behaviors. ASD affect 1% of the population, with males being affected four times more often than females¹⁻³. Family and twin studies indicate a strong genetic basis for ASD, but the mechanisms of transmission remain largely unknown. Recently, several synaptic genes have been associated with ASD, providing a better idea of the pathways involved⁴. The 22q13 deletion syndrome is characterized by developmental delay, moderate to profound language delay, delay/absence of expressive speech, hypotonia and autistic features that are caused by the loss of the *SHANK3* gene located at the tip of this chromosome⁵. The *SHANK3* gene can also be altered in patients with ASD, and recently, we have shown that mutations, or the loss of one copy of *SHANK3*, are associated with autism, whereas the presence of an extra copy of *SHANK3* might be associated with Asperger syndrome⁶. The variations identified included *de novo* deleterious mutations and inherited non-synonymous variations affecting highly conserved amino acids in the ankyrin domain^{6,7}. Although these mutations were inherited from healthy parents, they could contribute to the disorder in combination with other unidentified *SHANK3* mutations or in combination with other mutated genes.

The three members of the Shank family (Shank1, 2 and 3) are core components of the post-synaptic density (PSD), a highly organized cytoskeletal structure found adjacent to the postsynaptic membrane of excitatory synapses. Shank proteins have ankyrin repeats at their N-terminus, followed by a SH3 domain, a PDZ domain, a proline-rich region and a SAM domain at their C-terminal region⁸⁻¹⁰. All of these domains are involved in protein-protein interactions, linking different glutamate receptors, scaffolding proteins and intracellular effectors to the actin cytoskeleton. Indeed, Shank proteins are associated with NMDA receptors via the GKAP/PSD-95 complex and with type I metabotropic glutamate receptors via Homer in the proline-rich domain^{8,11,12}. In addition, Shank proteins can bind to several actin-regulatory molecules, such as cortactin^{13,14}, Sharpin¹⁵, α -fodrin¹⁶, Abp1¹⁷, β -Pix¹⁸ and SPAR¹⁹. The actin cytoskeleton of the dendritic spine is particularly dynamic and plays a pivotal role in the formation and the maturation of spines and is also involved in the

morphological changes that occur in spines during synaptic plasticity²⁰. Thus, Shank proteins and their binding partners are involved *in vitro* in the regulation of the size and the shape of dendritic spine²¹⁻²³.

To further assess the functional consequences of *SHANK3* mutations, we used an overexpression approach in cultured neurons to investigate the molecular mechanisms modulated by Shank3 in synapse formation and axonal outgrowth. We first examined the subcellular localization of the wild-type and mutated Shank3 proteins in fibroblasts and embryonic primary neuronal cultures. Our results show that the truncating mutation strongly affected spine development and morphology, as well as growth cone motility, whereas the *de novo* mutation Q321R preferentially had an effect in early stages of development. Finally, inherited mutations (R12C and R300C) displayed an intermediate phenotype, with lowered spine induction and maturation and growth cone motility compared with wild-type Shank3.

Materials and methods

DNA constructs

Full-length rat *Shank3* cDNA has been used previously⁶. Mutated forms (GFP-Shank3^{R12C}, GFP-Shank3^{R300C} and GFP-Shank3^{Q321R}) of GFP-Shank3 were generated using the QuikChange Site-Directed Mutagenesis Kit (Stratagene). Deletion variants of GFP-Shank3^{STOP} were made by introducing a STOP codon by direct mutagenesis to generate Shank3 mutants lacking the C-terminal part of the protein, corresponding to the mutation frameshift 3915 identified in patients. The monomeric red fluorescent protein (mRFP) construct was generously provided by I. Macara (University of Virginia, Charlottesville, VA). C. Gauthier-Rouviere (Centre de Recherche en Biochimie Macromoléculaire, Centre National de la Recherche Scientifique Montpellier, France) generously provided the red fluorescent protein RFP-actin construct. The SureSilencing short-hairpin RNA (shRNA) plasmids cloned in p-RFP-C-RS were purchased from Origene. Details of the downregulation experiments are described in the supplementary note.

Antibodies

Primary antibodies were anti-actin (Cytoskeleton), β -tubulin (Tuj-1, Covance), MAP2 (Chemicon), anti-DsRED (Clontech), anti-GFP (Invitrogen), anti-phospho-paxillin (Cell Signaling), anti-Shank3 (NeuroMab Facility), anti-cortactin and anti-vinculin (Sigma-Aldrich). Alexa Fluor 546 and 647 phalloidin were used to stain F-actin (Invitrogen). Secondary antibodies were conjugated to Alexa Fluor 488, 546 and 647 (Invitrogen).

Cell culture and transfection

HEK293T and COS-7 cells used for transient transfection were maintained in DMEM supplemented with fetal calf serum and antibiotics. Cells were transfected using calcium phosphate as previously described²⁴. Hippocampal neuronal cultures were prepared and transfected with the different constructs using the calcium phosphate method^{24,25}.

Immunocytochemistry

After four days, cells were fixed with 4% PFA, washed, permeabilized with 0.1% Triton/PBS or 0.05% Saponin/PBS, blocked for 1 hr with 10% NGS or 3% BSA before incubating for 1.5 hr with primary antibodies at room temperature in 3% NGS/PBS or in 0.2% BSA/PBS, then washed in PBS, and incubated with secondary antibodies in 3% NGS/PBS or in 0.2% BSA/PBS. Then, phalloidin was incubated 1 hr in 0.2% BSA/PBS.

Protein, western blots, immunoprecipitation

Protein preparation, western blots and immunoprecipitation were performed as described²⁶ and detailed in the supplementary note.

Ratio of F- to G-actin

The amount of F-actin and G-actin was measured with an Actin Polymerization Assay kit (BK037-Cytoskeleton). HEK293T cells were co-transfected with RFP-actin and GFP-C3 (control) or GFP-Shank3^{WT} or GFP-Shank3^{STOP}. Two days after transfection, the cells were resuspended in F-actin stabilization buffer with ATP (1 mM) and protease inhibitors (10X). To preserve F-actin, experiments were performed at 37°C. F-actin was pelleted by a 1-hr centrifugation at 100,000 x g, and the supernatant (G-actin) was separated. The pellet was resuspended in the same volume as the supernatant using ice-cold Milli-Q water and 10 μ M cytochalasin D for 2 hr at 4°C. Actin was

quantified by western blot using an anti-actin antibody (Cytoskeleton). The ratio of F-actin to G-actin was determined using an Odyssey infrared imaging system (LI-COR Biosciences).

Microscopy and quantitative analyses of spine morphology

Confocal images were acquired with a Leica DMR TCS SP2 AOBS confocal microscope, using the 60x objective. Each image was a z-series projection taken at 0.02- μm -deep intervals. The morphometric measurements (width and length of spine) were made using Volocity analysis software. Each experiment was performed on five to seven independent neuronal preparations. Cells were co-transfected with mRFP to visualize detailed morphology and to outline the spines. To determine spine size, 1500–1800 spines (from 16–28 neurons) were measured for each condition. For spine length, the distance from the base of the neck to the spine head was measured, and for spine width, the maximal width of the spine head perpendicular to the length was measured. To determine spine density, 10 regions of 20 μm were averaged per neuron.

To quantify F-actin and cortactin in spines, immunofluorescence images were acquired on a DM6000 Leica microscope equipped with MetaMorph software (Universal Imaging). The fluorescence intensity of F-actin or cortactin was measured as the average intensity in the manually area-represented head of the spine. Each experiment was performed on four to six independent neuronal preparations, and 20–38 neurons were measured for each condition.

Electrophysiology

Neurons (DIV17) co-transfected with GFP and the plasmids of interest were selected based on their fluorescence, and miniature EPSCs (mEPSCs) were recorded as previously published²². Briefly, the recording pipettes had a resistance of 5–10 MW when filled with the following medium (in mM): 140 CsCl, 0.5 CaCl₂, 20 EGTA, 10 HEPES, 10 D-glucose, pH 7.2 and osmolarity of 300 mOsm. The high concentration of EGTA avoided slow Ca²⁺-dependent desensitization of NMDARs²⁷. Neurons were perfused continuously with the following external medium (in mM): 140 NaCl, 2 CaCl₂, 3 KCl, 10 HEPES, 10 D-glucose, 0.01 glycine, 0.01 bicuculline, 0.0003 tetrodotoxin, pH 7.4 and osmolarity of 330 mOsm.

Live Imaging

Four days after transfection, approximately 10 growth cones of neurons transfected at DIV2 were analyzed by imaging every 2 seconds for 10 minutes with an Olympus IX71 inverted microscope (Olympus) using a 60x oil immersion objective (n = 35–67 growth cones from five independent experiments). The growth cone motility index was calculated as previously described²⁸.

Statistical significance

Data are shown as the mean \pm SEM. The statistical significance of the results was analyzed using one-way ANOVA in all experiments. For electrophysiological studies, we used the non-parametric Kruskal & Wallis test for more than two independent small samples.

Results

One of the aims of this study was to evaluate the contribution of *Shank3* gene mutations to the actin dynamics-dependent formation of dendritic spines. For this purpose, we studied *SHANK3* mutations identified in patients with ASD^{6,7}. Among these mutations (Figure 1a), one is a frameshift mutation at position 3680 in human *SHANK3* cDNA (3915 in rat), which introduces a premature STOP codon at position 1227 in humans (1304 in rat) leading to a truncated form of Shank3 (Shank3^{STOP}). The remaining three mutations are non-synonymous mutations located in or near the highly conserved ankyrin domain (R12C, R300C and Q321R, referred to as Shank3^{R12C}, Shank3^{R300C} and Shank3^{Q321R}, respectively)^{6,7}. An immunoblot analysis of the different constructs revealed that the fusion proteins carrying the point mutations Shank3^{R12C}, Shank3^{R300C} and Shank3^{Q321R} had similar levels of expression and size as the GFP-Shank3^{WT}, whereas the frameshift mutation (Shank3^{STOP}) led to a shorter protein (Figure 1b).

Decreased clustering of mutated Shank3 at the tips of actin filaments

We first analyzed the intracellular localization of Shank3^{WT} in COS-7 cells (Figure 1c). Shank3^{WT} was found at the plasma membrane and in large intracellular clusters, as previously reported in HEK cells²⁹. Interestingly, we noticed that Shank3 clustered at the tips of actin filaments and co-localized

with vinculin or phospho-paxillin, two focal adhesion proteins (Figure 1c). Overexpression of Shank3^{R12C}, Shank3^{R300C} and Shank3^{Q321R} in COS-7 showed that mutations in the ankyrin domain did not affect the localization of Shank3 at the membrane or in intracellular clusters (Figure 1d). However, the distribution of Shank3^{STOP} was restricted to small aggregates around the nucleus, suggesting that the lack of the C-terminus in Shank3 affected its targeting and its interaction with the actin cytoskeleton in COS-7 cells. The analysis of the co-localization of Shank3 with actin stress fibers showed that 60±2% of actin filaments per cell had clusters of Shank3^{WT}. Mutations in the ankyrin domain (R12C, R300C, and Q321R) significantly reduced this localization of Shank3 (43±3% for Shank3^{R12C}, 42±3% for Shank3^{R300C}, ***p<0.001, 48±3% for Shank3^{Q321R}, *p<0.05; Figure 1e). Shank3^{STOP} was almost completely absent at the tips of actin filaments (10±7% for Shank3^{STOP}, ***p<0.001).

Shank3 binds actin and positively affects actin polymerization

Because Shank proteins and their partners are involved in actin regulation^{13,18,30} and Shank3 co-localizes with actin fibers, we performed a co-immunoprecipitation using hippocampal tissue to demonstrate the existence of Shank3–actin complexes *in vivo* (Figure 1f). In addition, we used an actin polymerization assay to measure and compare the F- to G-actin ratio in GFP-Shank3– or GFP-C3–transfected cells (Figure 1g-h). In this assay, RFP-actin was co-transfected with each construct to stimulate actin polymerization. We analyzed the Shank3^{STOP} construct because this mutated protein does not co-localize with actin filaments. Overexpression of Shank3^{WT} significantly increased the amount of F-actin (1.399±0.039) compared with the control (***p<0.001; Figure 1g-h), showing the role of Shank3^{WT} in *in vitro* actin polymerization. In contrast, no significant difference in actin polymerization was observed with Shank3^{STOP} protein (0.971±0.062; p>0.05) compared with the control. These results suggest that the C-terminus of Shank3 is crucial for actin dynamics.

Shank3 mutations affect spine induction and spine morphology

To analyze the role of Shank3 in actin cytoskeleton regulation in dendritic spines, we overexpressed the different constructs in hippocampal neurons and studied their effects on the organization and shape of postsynaptic spines. First, we analyzed the subcellular localization of the different Shank3 mutants

co-transfected with an RFP plasmid in hippocampal neurons. Shank3^{WT} overexpression led to an accumulation of the protein in dendritic spines (Figure 2a), as previously reported³¹. Point mutations (Shank3^{R12C}, Shank3^{R300C} and Shank3^{Q321R}) did not affect this synaptic targeting. As observed in COS-7 cells, Shank3^{STOP} accumulated in the soma, was weakly localized in the dendrites and was absent from dendritic spines, indicating that the C-terminus was required for the dendritic targeting of Shank3. These results are consistent with previous data showing that the Homer binding site is involved in the synaptic localization of Shank3^{22,31}.

In addition, Shank3^{WT} significantly increased the number of spines compared with the control (Figure 2b) and reduced the number of filopodia (Figure 2c) in rat hippocampal neurons. The number of spines per 20 μm of dendrite length was 6.3 ± 0.4 spines when Shank3^{WT} was overexpressed, compared with 3.4 ± 0.3 spines in control GFP-positive neurons ($***p < 0.001$). Overexpression of Shank3^{R12C}, Shank3^{R300C} or Shank3^{Q321R} also increased the number of spines, but not as much as Shank3^{WT} (4.6 ± 0.3 , 4.7 ± 0.3 , or 5.0 ± 0.2 spines per 20 μm , respectively; $**p < 0.01$ and $***p < 0.001$ compared with control). The mutations in the ankyrin domain therefore had moderate effects on spine induction, but still significantly lower than Shank3^{WT} ($^{\circ}p < 0.05$; $^{\circ\circ}p < 0.01$ and $^{\circ\circ\circ}p < 0.001$, respectively). The overexpression of Shank3^{STOP} had a stronger effect, with a reduction in the number of spines compared with Shank3^{WT} and with the control (2.6 ± 0.2 spines per 20 μm ; $^{\circ\circ\circ}p < 0.001$ compared with Shank3^{WT} and $*p < 0.05$ compared with the control). **Moreover, a Sh-resistant form of Shank3^{STOP} did not rescue the spine phenotype in hippocampal neurons where Shank3 was down-regulated (supplementary figure 1).** Altogether, our results suggest that Shank3^{STOP} has a dominant-negative effect on spine induction in a wild-type background, probably by affecting the targeting and/or the stability of the wild-type protein at synapses.

Finally, we investigated the impact of Shank3 mutations on spine maturation and measured spine head enlargement and spine length from the base to the top of the head in rat hippocampal neurons transfected with each construct (Figure 2d). The number of spines with head widths $> 0.5 \mu\text{m}$ was significantly increased in neurons transfected with Shank3^{WT} compared with neurons transfected with GFP ($63 \pm 3\%$ of spines $> 0.5 \mu\text{m}$ head width compared to $51 \pm 3\%$ of spines; $*p < 0.05$; Figure 2e-

f). No difference in spine length was observed (44±3% of spines > 1.0 μm length for the control and 41±3% of spines for Shank3^{WT}, Figure 2g). Thus, in mature neurons, Shank3 overexpression promoted the morphological maturation of spines, as previously observed with Shank3^{WT} expressed in aspiny neurons²² or with Shank1 in hippocampal cells²¹.

Compared with the control, Shank3^{STOP} did not change the width of spine heads (46.6±2% of spines > 0.5 μm; p>0.5) but reduced the length of the spines (34±2% of spines > 1.0 μm length; *p < 0.05). Shank3^{Q321R} showed a slight increase in the width of the spine head (59±2% of spines > 0.5 μm, ***p<0.001) and a reduction in spine length (34±2% of spines > 1.0 μm, *p<0.05). This suggests that the Q321R mutation does not abolish the effect of Shank3 on spine maturation but does affect neck retraction. Finally, Shank3^{R12C} and Shank3^{R300C} did not increase the size of spine-heads (54±4% and 51±3% of spines > 0.5 μm; p>0.05 compared with control), suggesting that these mutations disrupt the effect of Shank3 on spine morphology. Altogether, our data suggest that Shank3^{WT} overexpression promotes spine induction and maturation and that all mutations identified in ASD modify the function of Shank3.

Shank3 mutations affect F-actin content but not cortactin level in dendritic spines

As actin dynamics play key roles in dendrite development and specifically in spine formation and maturation^{32,33}, we further examined the effects of Shank3 mutations on the synaptic levels of F-actin and cortactin (Figure 3). Cortactin is an F-actin binding protein enriched in cell matrix contact sites that facilitates the nucleation of new actin branches at the tips of actin filaments. In mature neurons, F-actin appeared in the form of patches and puncta along the dendrites, and it was enriched in the heads of dendritic spines (Figure 3a). We quantified the level of actin in spine heads as a ratio of the average intensity of transfected neurons to untransfected neurons. We observed an increase in F-actin levels in the spines of Shank3^{WT}-transfected neurons compared with the control (147±8% for Shank3^{WT} and 109±6% for the control; ***p<0.001; Figure 3b), as previously described for Shank1²¹. Neurons transfected with Shank3^{R12C} and Shank3^{R300C} constructs displayed intermediate levels of F-actin between the control and Shank3^{WT} levels (123±7% for Shank3^{R12C}, 125±9% for Shank3^{R300C}). The absence of an increase in F-actin as large as that induced by Shank3^{WT} suggests that mutations in the

ankyrin domain affect F-actin content in dendritic spines. Neither the truncating mutation nor Shank3^{Q321R} increased F-actin level (93±6% for Shank3^{STOP} and 115±8% for Shank3^{Q321R}; °°°p<0.001 and °°p<0.01 compared to Shank3^{WT}). In the case of the truncating mutation, this was most likely due to a lack of targeting to the spines. Our data show that enlargement of dendritic spines induced by Shank3^{WT} was correlated with increases in F-actin level. The mutations in the ankyrin domain and the truncated form of Shank3 all affected spines maturation via an actin-dependent mechanism, as suggested by our fibroblast experiments (Figure 1).

Because Shank3 binds to cortactin and the loss of cortactin causes a decrease in spine density^{12,13,21}, we examined the effect of each mutation on cortactin content in dendritic spines. Despite Shank3 mutations significantly reducing the level of F-actin in spines, cortactin level was not significantly different between the control and Shank3^{WT} (Figure 3c, p>0.05).

The Shank3 mutations decrease spontaneous neuronal activity

Because the number and the morphology of spines might affect the strength of synaptic transmission, we further explored the functional consequences of Shank3 mutations by recording mEPSCs in hippocampal neurons. Shank3^{WT} had no significant effect on mEPSC amplitude but markedly increased mEPSC frequency compared with GFP-only neurons (1.48±0.08 and 0.74±0.08 Hz, respectively, ***p<0.001; Figure 4). The present correlation between Shank3^{WT}-mediated changes in spine morphology and electrical activity is in agreement with previous results²¹. Shank3^{R12C}, Shank3^{R300C} and Shank3^{Q321R} modestly increased mEPSC frequency, but not as much as Shank3^{WT} (0.98±0.16, 0.97±0.23, and 1.1±0.24 Hz, respectively; °p<0.05). In contrast, Shank3^{STOP} strongly reduced the frequency (0.50±0.17 Hz; °°°p<0.001) as well as the amplitude of mEPSCs compared with the control (Shank3^{STOP}, 15.90±0.72 pA; GFP-only 31.49±2.48 pA; ***p<0.001), extending the dominant-negative effect displayed by Shank3^{STOP} to the modulation of synaptic transmission.

The Q321R and STOP mutations affect growth cone motility induced by Shank3^{WT}

Q321R is a *de novo* mutation identified in a girl with autism, language delay and developmental delay⁷. Here we found that this mutation was associated with abnormalities in spine morphology (even if less pronounced than for Shank3^{STOP}). We then assessed whether Shank3 could play a role earlier in

neuronal development. Indeed, Shank3 is expressed in the brain at early stages³⁴, and Shank and cortactin are enriched within the lamellipodia of motile cells and in neuronal growth cones^{12,35}. We analyzed the localization of endogenous or overexpressed Shank3 in cultured hippocampal neurons by immunocytochemistry in early stages (Figure 5a-b). Endogenous Shank3 was detected in young neurons (day 2), and labeling with actin revealed the accumulation of the protein in ruffles. We also confirmed the co-localization of Shank3 and cortactin in axonal growth cones. Then, we tested whether Shank3 regulated growth cone dynamics by co-transfecting GFP-C3 with GFP-Shank3^{WT} or with the mutated forms in young hippocampal neurons. Four days after the transfection, live cell imaging was performed as described²⁸. The axonal growth cone motility was quantified as a dimensionless motility index (MI). We quantified the mean value of MI for 10–15 axonal growth cones for each construct (Figure 5c-d). We observed an increase of MI with Shank3^{WT} compared with the control (0.129±0.005 for Shank3^{WT} to 0.101±0.005 for GFP-C3; ***p<0.001). This suggests that full-length Shank3 induces higher axonal growth cone motility. We did not observe such an increase for GFP-Shank3^{Q321R} or GFP-Shank3^{STOP} (0.106±0.003 and 0.112±0.004; p<0.001). Together, these data suggest that these two *de novo* mutations, Shank3^{Q321R} and Shank3^{STOP}, affect neuronal motility during development.

Discussion

Three important conclusions can be drawn from this study. First, we found that Shank3 increases actin polymerization, promoting spine formation and increasing the frequency of mEPSPs. Second, we demonstrated that Shank3 mutations identified in ASD disrupt these processes, providing a cellular readout for Shank3-associated pathologies. Third, we described two *de novo* mutations, Shank3^{Q321R} and Shank3^{STOP}, associated with severe loss of function, and two inherited mutations, Shank3^{R12C} and Shank3^{R300C}, which produced an intermediate phenotype and might represent a risk factor for ASD.

Shank3 promotes spine formation and shape via an actin-dependent mechanism.

Spine structure is regulated by various molecular mechanisms, and actin polymerization is a crucial process for synaptic structure and function³⁶. Actin filaments in the spine head are highly dynamic and

regulate the molecular organization of the PSD and modulate postsynaptic signal transduction³⁷⁻³⁹. Our data on neuronal cultures show that Shank3 overexpression induces an increase in spine density associated with an F-actin accumulation and an increase in mEPSP frequency. These effects could be mediated in part by a regulation of capping proteins, as we demonstrated that Shank3 co-localized with vinculin and phospho-paxillin at the tip of actin stress fibers in fibroblasts. These capping proteins control the growth of actin filaments in lamellipodia, resulting in filopodia formation and a reduction in lamellipodia⁴⁰. In mature neurons, they localize throughout dendritic spines⁴¹, similar to Shank3. Furthermore, the Shank complex could be linked to several other proteins regulating actin cytoskeleton dynamics, such as β -Pix, a guanine nucleotide exchange factor for Rac1 and cdc42 small GTPases¹⁸; Abp1, a member of the Arp2/3 complex¹⁷; and cortactin³⁵. Indeed, depletion of the Arp2/3 complex, including cortactin, Abi2, WAVE-1, N-WASP, and Abp1, alters the morphology and number of spines^{13,42-45}. Altogether, these results suggest that Shank3 could directly regulate F-actin level in spines, resulting in a modification of the shape and the function of these spines.

In this study, we observed increased spine density and morphology with Shank3, which is consistent with previous results obtained in aspiny neurons with Shank3²². Shank1B induces an enlargement of spine heads independent of spine density, and this enlargement is enhanced by co-expression of the long form of Homer^{21,43,46}. Recent data on Shank1 knock-out mice suggest that Shank1 is not required for spine formation but promotes the growth and stability of large spines, which is consistent with *in vitro* results⁴⁷. Shank2 also affects spine head maturation, depending on the Arp2/3 complex³⁰. Therefore, it is now clearly established that Shank proteins are involved in spinogenesis, especially in spine maturation, and we highlighted in this study that this occurs via an actin-dependent mechanism.

Shank3 mutations associated with ASD disrupt its cellular functions

We showed that *de novo* or inherited Shank3 mutations associated with ASD can affect its localization at the tip of the F-actin fibers, subsequently disrupting spine formation and morphology. This effect was especially strong for Shank3^{STOP} and was similar to that observed in hippocampal neurons where Shank3 was downregulated (this study and ref23) or in cerebellar neurons transfected with Shank3

bearing a mutation in the Homer binding site²². This mutation appears to have a dominant-negative effect on the induction and the maturation of spines in a wild-type background (Figure 2b). **This could be due to interference with the localization of other binding partners and/or to PDZ domain dimerization of the mutated form with the endogenous Shank3⁴⁸.**

Our results highlight the potential impact of the two *de novo* mutations of Shank3 on early stages of neuronal development. We showed that the endogenous as well as the overexpressed Shank3 was localized in the growth cones of young neurons, suggesting that Shank3 could participate in neurite extension. Consistent with this idea, cortactin mediates neurite outgrowth¹³, and the depletion of Abp1, a linker of Shank3 to the actin complex, results in increased axon length in early stages of neuronal development⁴⁹. The Shank3^{STOP} and Shank3^{Q321R} *de novo* mutations decreased growth cone motility, which could lead to disrupted connectivity in patients carrying either mutation. These results are consistent with a recent study showing that the lack of C-terminal domains (including Homer and cortactin binding sites and the SAM domain) inhibits the induction of neurite outgrowth⁵⁰.

Inherited mutations represent risk factors for ASD

Mutations in *SHANK3*, including *de novo* mutations, *de novo* copy number variations and inherited mutations, have been frequently reported in patients^{6,7,50}. The importance of the Shank family for ASD was further strengthened by the recent identification of mutations in *SHANK2* in ASD patients^{51,52}. If the impact of *de novo* deleterious mutations is well established, the role of inherited mutations remains unclear. **Here, we showed that the two inherited mutations, Shank3^{R12C} and Shank3^{R300C}, have intermediate effects, mainly on spine formation.** These results suggest that despite their transmission from healthy parents, these mutations could cause subtle synaptic defects increasing the risk of developing ASD. *SHANK3* mutations can also be involved in other neurologic disorders, such as intellectual disability and schizophrenia⁵⁰. In the case of schizophrenia, the *de novo* mutation R1117X with germline mosaicism has been observed in three affected brothers. They presented mild to moderate intellectual disability and schizoaffective disorder, but no evidence of autistic features. Functional studies have confirmed that this mutation causes a loss of *SHANK3* function in zebrafish and decreases neurite outgrowth in mice⁵⁰. It is unclear how similar mutations can lead to different

clinical conditions. The same is true for mutations in *NLGN3* and *NLGN4* described in autism but also in intellectual disability, Asperger syndrome, and Tourette syndrome with hyperactivity disorder⁵³⁻⁵⁵. Mutations in *NRXN1* have also been observed in patients with schizophrenia and in asymptomatic carriers⁵⁶. These different outcomes could be due to mutations altering either all or specific roles of these proteins (e.g., axonal guidance, synapse formation). We can also expect that additional genetic/epigenetic and environmental risk factors acting at different levels of brain development could bias the phenotype towards different sets of disorders⁵⁷. The identification of such factors would allow us to better understand the nature of the biological mechanisms underlying these different disorders and to provide insight for new treatments.

Supplementary information

Supplementary information is available at Molecular Psychiatry's website

Acknowledgements

We thank I. Macara for providing the mRFP construct and C. Gauthier-Rouviere for the mRFP-actin construct. We thank Julien Bensalem, Marie-Claude Donat, Lea Lasvaux, and Chantal Medina for technical assistance; we thank Drs Jerome Ezan, Roberto Toro and Claudia Racca for helpful comments and discussion.

This work was supported by INSERM AVENIR grant to N.S. and M.M., Conseil Régional d'Aquitaine (NS, MM), La Fondation pour la Recherche Medicale (NS, MM), La Fondation Jerome Lejeune (NS), FRM and Orange fellowships (CD) and the European Commission Coordination Action ENINET (contract number LSHM-CT-2005-19063; NS & MM). The sequencing was performed at the Sequencing facility of Bordeaux (grants from the Conseil Régional d'Aquitaine n° 20030304002FA and 20040305003FA and from the European Union, FEDER n° 2003227). The confocal microscopy was done at the Bordeaux Imaging Center of the Neurosciences Institute of the University of Bordeaux II. The monoclonal antibody against Shank3 was developed by and obtained from the UC Davis/NINDS/NIMH NeuroMab Facility, supported by NIH grant U24NS050606 and maintained by the Department of Pharmacology, School of Medicine, University of California, Davis, CA 95616.

Conflict of interest

The authors declare no conflict of interest.

References

1. Chakrabarti S, Fombonne E. Pervasive developmental disorders in preschool children: confirmation of high prevalence. *Am J Psychiatry* 2005; **162**(6): 1133-1141.
2. Newschaffer CJ, Croen LA, Daniels J, Giarelli E, Grether JK, Levy SE *et al.* The epidemiology of autism spectrum disorders. *Annu Rev Public Health* 2007; **28**: 235-258.
3. Baird G, Simonoff E, Pickles A, Chandler S, Loucas T, Meldrum D *et al.* Prevalence of disorders of the autism spectrum in a population cohort of children in South Thames: the Special Needs and Autism Project (SNAP). *Lancet* 2006; **368**(9531): 210-215.
4. Toro R, Konyukh M, Delorme R, Leblond C, Chaste P, Fauchereau F *et al.* Key role for gene dosage and synaptic homeostasis in autism spectrum disorders. *Trends Genet* 2010; **26**(8): 363-372.
5. Bonaglia MC, Giorda R, Borgatti R, Felisari G, Gagliardi C, Selicorni A *et al.* Disruption of the ProSAP2 gene in a t(12;22)(q24.1;q13.3) is associated with the 22q13.3 deletion syndrome. *American journal of human genetics* 2001; **69**(2): 261-268.
6. Durand CM, Betancur C, Boeckers TM, Bockmann J, Chaste P, Fauchereau F *et al.* Mutations in the gene encoding the synaptic scaffolding protein SHANK3 are associated with autism spectrum disorders. *Nature genetics* 2007; **39**(1): 25-27.
7. Moessner R, Marshall CR, Sutcliffe JS, Skaug J, Pinto D, Vincent J *et al.* Contribution of SHANK3 mutations to autism spectrum disorder. *American journal of human genetics* 2007; **81**(6): 1289-1297.
8. Sheng M, Kim E. The Shank family of scaffold proteins. *Journal of cell science* 2000; **113** (Pt 11): 1851-1856.
9. Boeckers TM, Bockmann J, Kreutz MR, Gundelfinger ED. ProSAP/Shank proteins - a family of higher order organizing molecules of the postsynaptic density with an emerging role in human neurological disease. *J Neurochem* 2002; **81**(5): 903-910.
10. Baron MK, Boeckers TM, Vaida B, Faham S, Gingery M, Sawaya MR *et al.* An architectural framework that may lie at the core of the postsynaptic density. *Science* 2006; **311**(5760): 531-535.
11. Boeckers TM, Winter C, Smalla KH, Kreutz MR, Bockmann J, Seidenbecher C *et al.* Proline-rich synapse-associated proteins ProSAP1 and ProSAP2 interact with synaptic proteins of the SAPAP/GKAP family. *Biochemical and biophysical research communications* 1999; **264**(1): 247-252.
12. Naisbitt S, Kim E, Tu JC, Xiao B, Sala C, Valtschanoff J *et al.* Shank, a novel family of postsynaptic density proteins that binds to the NMDA receptor/PSD-95/GKAP complex and cortactin. *Neuron* 1999; **23**(3): 569-582.
13. Hering H, Sheng M. Activity-dependent redistribution and essential role of cortactin in dendritic spine morphogenesis. *J Neurosci* 2003; **23**(37): 11759-11769.
14. Uruno T, Liu J, Zhang P, Fan Y, Egile C, Li R *et al.* Activation of Arp2/3 complex-mediated actin polymerization by cortactin. *Nature cell biology* 2001; **3**(3): 259-266.

15. Lim S, Sala C, Yoon J, Park S, Kuroda S, Sheng M *et al.* Sharpin, a novel postsynaptic density protein that directly interacts with the shank family of proteins. *Molecular and cellular neurosciences* 2001; **17**(2): 385-397.
16. Bockers TM, Mameza MG, Kreutz MR, Bockmann J, Weise C, Buck F *et al.* Synaptic scaffolding proteins in rat brain. Ankyrin repeats of the multidomain Shank protein family interact with the cytoskeletal protein alpha-fodrin. *The Journal of biological chemistry* 2001; **276**(43): 40104-40112.
17. Qualmann B, Boeckers TM, Jeromin M, Gundelfinger ED, Kessels MM. Linkage of the actin cytoskeleton to the postsynaptic density via direct interactions of Abp1 with the ProSAP/Shank family. *J Neurosci* 2004; **24**(10): 2481-2495.
18. Park E, Na M, Choi J, Kim S, Lee JR, Yoon J *et al.* The Shank family of postsynaptic density proteins interacts with and promotes synaptic accumulation of the beta PIX guanine nucleotide exchange factor for Rac1 and Cdc42. *The Journal of biological chemistry* 2003; **278**(21): 19220-19229.
19. Wendholt D, Spilker C, Schmitt A, Dolnik A, Smalla KH, Proepper C *et al.* ProSAP-interacting protein 1 (ProSAPiP1), a novel protein of the postsynaptic density that links the spine-associated Rap-Gap (SPAR) to the scaffolding protein ProSAP2/Shank3. *The Journal of biological chemistry* 2006; **281**(19): 13805-13816.
20. Sekino Y, Kojima N, Shirao T. Role of actin cytoskeleton in dendritic spine morphogenesis. *Neurochem Int* 2007; **51**(2-4): 92-104.
21. Sala C, Piech V, Wilson NR, Passafaro M, Liu G, Sheng M. Regulation of dendritic spine morphology and synaptic function by Shank and Homer. *Neuron* 2001; **31**(1): 115-130.
22. Roussignol G, Ango F, Romorini S, Tu JC, Sala C, Worley PF *et al.* Shank expression is sufficient to induce functional dendritic spine synapses in aspiny neurons. *J Neurosci* 2005; **25**(14): 3560-3570.
23. Grabrucker AM, Knight MJ, Proepper C, Bockmann J, Joubert M, Rowan M *et al.* Concerted action of zinc and ProSAP/Shank in synaptogenesis and synapse maturation. *Embo J* 2011; **30**(3): 569-581.
24. Sans N, Wang PY, Du Q, Petralia RS, Wang YX, Nakka S *et al.* mPins modulates PSD-95 and SAP102 trafficking and influences NMDA receptor surface expression. *Nature cell biology* 2005; **7**(12): 1179-1190.
25. Sans N, Prybylowski K, Petralia RS, Chang K, Wang YX, Racca C *et al.* NMDA receptor trafficking through an interaction between PDZ proteins and the exocyst complex. *Nature cell biology* 2003; **5**(6): 520-530.
26. Sans N, Petralia RS, Wang YX, Blahos J, 2nd, Hell JW, Wenthold RJ. A developmental change in NMDA receptor-associated proteins at hippocampal synapses. *J Neurosci* 2000; **20**(3): 1260-1271.
27. Medina I, Filippova N, Bakhrarov A, Bregestovski P. Calcium-induced inactivation of NMDA receptor-channels evolves independently of run-down in cultured rat brain neurones. *J Physiol* 1996; **495** (Pt 2): 411-427.
28. Ibarretxe G, Perrais D, Jaskolski F, Vimeney A, Mulle C. Fast regulation of axonal growth cone motility by electrical activity. *J Neurosci* 2007; **27**(29): 7684-7695.

29. Quitsch A, Berhorster K, Liew CW, Richter D, Kreienkamp HJ. Postsynaptic shank antagonizes dendrite branching induced by the leucine-rich repeat protein Densin-180. *J Neurosci* 2005; **25**(2): 479-487.
30. Haeckel A, Ahuja R, Gundelfinger ED, Qualmann B, Kessels MM. The actin-binding protein Abp1 controls dendritic spine morphology and is important for spine head and synapse formation. *J Neurosci* 2008; **28**(40): 10031-10044.
31. Boeckers TM, Liedtke T, Spilker C, Dresbach T, Bockmann J, Kreutz MR *et al.* C-terminal synaptic targeting elements for postsynaptic density proteins ProSAP1/Shank2 and ProSAP2/Shank3. *J Neurochem* 2005; **92**(3): 519-524.
32. Caceres A, Payne MR, Binder LI, Steward O. Immunocytochemical localization of actin and microtubule-associated protein MAP2 in dendritic spines. *Proc Natl Acad Sci U S A* 1983; **80**(6): 1738-1742.
33. Tada T, Sheng M. Molecular mechanisms of dendritic spine morphogenesis. *Current opinion in neurobiology* 2006; **16**(1): 95-101.
34. Petralia RS, Sans N, Wang YX, Wenthold RJ. Ontogeny of postsynaptic density proteins at glutamatergic synapses. *Molecular and cellular neurosciences* 2005; **29**(3): 436-452.
35. Du Y, Weed SA, Xiong WC, Marshall TD, Parsons JT. Identification of a novel cortactin SH3 domain-binding protein and its localization to growth cones of cultured neurons. *Molecular and cellular biology* 1998; **18**(10): 5838-5851.
36. Cingolani LA, Goda Y. Actin in action: the interplay between the actin cytoskeleton and synaptic efficacy. *Nat Rev Neurosci* 2008; **9**(5): 344-356.
37. Kuriu T, Inoue A, Bito H, Sobue K, Okabe S. Differential control of postsynaptic density scaffolds via actin-dependent and -independent mechanisms. *J Neurosci* 2006; **26**(29): 7693-7706.
38. Star EN, Kwiatkowski DJ, Murthy VN. Rapid turnover of actin in dendritic spines and its regulation by activity. *Nat Neurosci* 2002; **5**(3): 239-246.
39. Honkura N, Matsuzaki M, Noguchi J, Ellis-Davies GC, Kasai H. The subspine organization of actin fibers regulates the structure and plasticity of dendritic spines. *Neuron* 2008; **57**(5): 719-729.
40. Mejillano MR, Kojima S, Applewhite DA, Gertler FB, Svitkina TM, Borisy GG. Lamellipodial versus filopodial mode of the actin nanomachinery: pivotal role of the filament barbed end. *Cell* 2004; **118**(3): 363-373.
41. Korobova F, Svitkina T. Molecular architecture of synaptic actin cytoskeleton in hippocampal neurons reveals a mechanism of dendritic spine morphogenesis. *Mol Biol Cell* 2010; **21**(1): 165-176.
42. Grove M, Demyanenko G, Echarri A, Zipfel PA, Quiroz ME, Rodriguiz RM *et al.* ABI2-deficient mice exhibit defective cell migration, aberrant dendritic spine morphogenesis, and deficits in learning and memory. *Molecular and cellular biology* 2004; **24**(24): 10905-10922.

43. Kim DJ, Kim SH, Lim CS, Choi KY, Park CS, Sung BH *et al.* Interaction of SPIN90 with the Arp2/3 complex mediates lamellipodia and actin comet tail formation. *The Journal of biological chemistry* 2006; **281**(1): 617-625.
44. Soderling SH, Guire ES, Kaech S, White J, Zhang F, Schutz K *et al.* A WAVE-1 and WRP signaling complex regulates spine density, synaptic plasticity, and memory. *J Neurosci* 2007; **27**(2): 355-365.
45. Wegner AM, Nebhan CA, Hu L, Majumdar D, Meier KM, Weaver AM *et al.* N-wasp and the arp2/3 complex are critical regulators of actin in the development of dendritic spines and synapses. *The Journal of biological chemistry* 2008; **283**(23): 15912-15920.
46. Sala C, Futai K, Yamamoto K, Worley PF, Hayashi Y, Sheng M. Inhibition of dendritic spine morphogenesis and synaptic transmission by activity-inducible protein Homer1a. *J Neurosci* 2003; **23**(15): 6327-6337.
47. Hung AY, Futai K, Sala C, Valtschanoff JG, Ryu J, Woodworth MA *et al.* Smaller dendritic spines, weaker synaptic transmission, but enhanced spatial learning in mice lacking Shank1. *J Neurosci* 2008; **28**(7): 1697-1708.
48. Iskenderian-Epps WS, Imperiali B. Modulation of Shank3 PDZ domain ligand-binding affinity by dimerization. *Chembiochem* 2010; **11**(14): 1979-1984.
49. Pinyol R, Haeckel A, Ritter A, Qualmann B, Kessels MM. Regulation of N-WASP and the Arp2/3 complex by Abp1 controls neuronal morphology. *PLoS One* 2007; **2**(5): e400.
50. Gauthier J, Champagne N, Lafreniere RG, Xiong L, Spiegelman D, Brustein E *et al.* De novo mutations in the gene encoding the synaptic scaffolding protein SHANK3 in patients ascertained for schizophrenia. *Proc Natl Acad Sci U S A* 2010; **107**(17): 7863-7868.
51. Berkel S, Marshall CR, Weiss B, Howe J, Roeth R, Moog U *et al.* Mutations in the SHANK2 synaptic scaffolding gene in autism spectrum disorder and mental retardation. *Nature genetics* 2010; **42**(6): 489-491.
52. Pinto D, Pagnamenta AT, Klei L, Anney R, Merico D, Regan R *et al.* Functional impact of global rare copy number variation in autism spectrum disorders. *Nature* 2010; **466**(7304): 368-372.
53. Jamain S, Quach H, Betancur C, Rastam M, Colineaux C, Gillberg IC *et al.* Mutations of the X-linked genes encoding neuroligins NLGN3 and NLGN4 are associated with autism. *Nature genetics* 2003; **34**(1): 27-29.
54. Laumonier F, Bonnet-Brilhault F, Gomot M, Blanc R, David A, Moizard MP *et al.* X-linked mental retardation and autism are associated with a mutation in the NLGN4 gene, a member of the neuroligin family. *American journal of human genetics* 2004; **74**(3): 552-557.
55. Lawson-Yuen A, Saldivar JS, Sommer S, Picker J. Familial deletion within NLGN4 associated with autism and Tourette syndrome. *Eur J Hum Genet* 2008; **16**(5): 614-618.
56. Zweier C, de Jong EK, Zweier M, Orrico A, Ousager LB, Collins AL *et al.* CNTNAP2 and NRXN1 are mutated in autosomal-recessive Pitt-Hopkins-like mental retardation and determine the level of a common synaptic protein in Drosophila. *American journal of human genetics* 2009; **85**(5): 655-666.

57. Cook EH, Jr., Scherer SW. Copy-number variations associated with neuropsychiatric conditions. *Nature* 2008; **455**(7215): 919-923.

Legends

Figure 1: Mutations in Shank3 affect its recruitment to the tips of actin filaments and actin polymerization.

(a) Localization of rare non-synonymous variations or truncating *SHANK3* mutations identified in ASD^{6,7}. ANK: ankyrin repeats; SH3: Src homology 3 domain; PDZ: postsynaptic density 95/Discs large/zona occludens-1 homology domain; Hbs: Homer binding site; Cbs: Cortactin binding site; SAM: sterile alpha motif domain. **(b)** Western blot analysis of the GFP constructs expressed in HEK293T cells. We observed similar sizes of Shank3^{WT} and fusion proteins carrying point mutations (Shank3^{R12C}, Shank3^{R300C}, and Shank3^{Q321R}). The frameshift mutation results in a truncated protein (222 kDa GFP-Shank3^{WT}, 169 kDa GFP-Shank3^{STOP}). **(c)** Localization of Shank3^{WT} in COS-7 cells transiently transfected with GFP-Shank3^{WT} (green) and labeled with phalloidin 647 to visualize F-actin (blue) and with anti-vinculin or anti-phospho-paxillin (red), two focal adhesion proteins. Shank3^{WT} is located at the membrane and in intracellular clusters that co-localize with vinculin or phospho-paxillin at the tips of actin filaments. On the right side, magnification of representative stress fibers with clusters of Shank3^{WT}. **(d)** Localization of Shank3^{WT} and mutated forms in COS-7 cells. COS-7 cells transiently transfected with GFP-Shank3^{WT} or mutated forms (green) and labeled with phalloidin 546 to visualize F-actin (red) and DAPI to visualize the nucleus (blue). Shank3^{R12C}, Shank3^{R300C} and Shank3^{Q321R} are located at the membrane and in intracellular clusters. Conversely, Shank3^{STOP} is restricted to around the nucleus. **(e)** Quantification of the accumulation of GFP constructs at the tips of actin filaments. Percentage of filaments with Shank3 clusters per cell (%). This accumulation is significantly reduced with mutated Shank3 and absent with Shank3^{STOP} (n = 30-40 cells). Scale bars represent 15 μ m. **(f)** Co-immunoprecipitation of Shank3 and actin in an adult rat brain. Lysate (Input) was incubated with control IgG or anti-Shank3. Immunoprecipitation was performed, followed by western blotting using anti- β -actin. **(g)** Shank3^{STOP} inhibits the effect of Shank3^{WT} on actin polymerization. HEK293T were transiently co-transfected with RFP-actin and GFP-C3 (control), GFP-Shank3^{WT}, or GFP-Shank3^{STOP}. Representative immunoblots of G-actin (G) and F-actin (F) fractions obtained with an Actin Polymerization Assay kit. G-actin and F-actin were probed with anti-actin antibody. **(h)** Ratio of F-actin/G-actin was measured for each condition. The

ratio is normalized to GFP-C3 and is represented as the mean \pm SEM. Shank3^{WT} enhances the polymerization of actin (**p<0.001; n = 6 independent experiments). Shank3^{STOP} inhibits the effect of Shank3 on actin polymerization.

Figure 2: Effect of Shank3^{WT} and mutants on dendritic spine induction and maturation. (a) Hippocampal neurons were transiently co-transfected with GFP-Shank3^{WT} or mutated forms (green) and RFP (red) and processed for immunofluorescence after 4 days (days *in vitro* 21, DIV21), and the subcellular localization of each construct was analyzed. Neurons are stained with anti-GFP (green) and anti-DsRED (red). Scale bars represent 20 μ m. On the bottom side, magnification of 20 μ m of the dendrite transfected with each construct. (b) Comparison of spine density in neurons transfected with the different Shank3 constructs (number of spines per 20 μ m of dendrite length) in co-transfected neurons. (c) Comparison of the density of filopodia (number of filopodia per 20 μ m of dendrite length) in co-transfected neurons. Shank3^{WT} leads to an increase in the number of spines and a decrease in the number of filopodia. All mutations reduce the ability of Shank3 to induce spines. (**p<0.001, *p<0.05 compared with the control; °°p<0.001, °p<0.01, °p<0.05 compared with Shank3^{WT}). (d) Examples of spines from neurons transfected with GFP-C3 or GFP-Shank3^{WT}. Spine length (green line) and head width (red line) were computed using Volocity software. (e) Truncating mutation causes a decrease in the number of larger spines and an increase in the number thin spines. Relative abundance of four different spine classes according to spine head size (0 to 0.25; 0.25 to 0.5; 0.5 to 0.75; and > 0.75 μ m). (f) Percentage of spine heads > 0.5 μ m within the same population. Spine heads are significantly larger in GFP-Shank3^{WT}- and GFP-Shank3^{Q321R}-transfected neurons compared with the control (**p<0.001, **p<0.01). Spine heads are significantly smaller in GFP-Shank3^{STOP}. (g) Percentage of spines of > 1.0 μ m within the same population. Spine length is significantly reduced with GFP-Shank3^{Q321R} and GFP-Shank3^{STOP} constructs compared with the control (*p<0.05; n= 17–28 neurons and 1500–1800 spines).

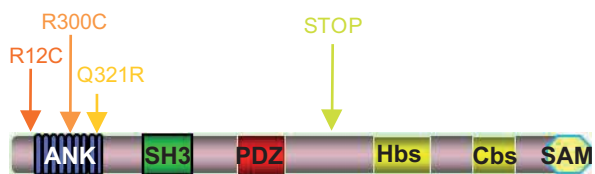
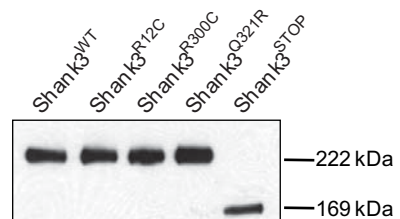
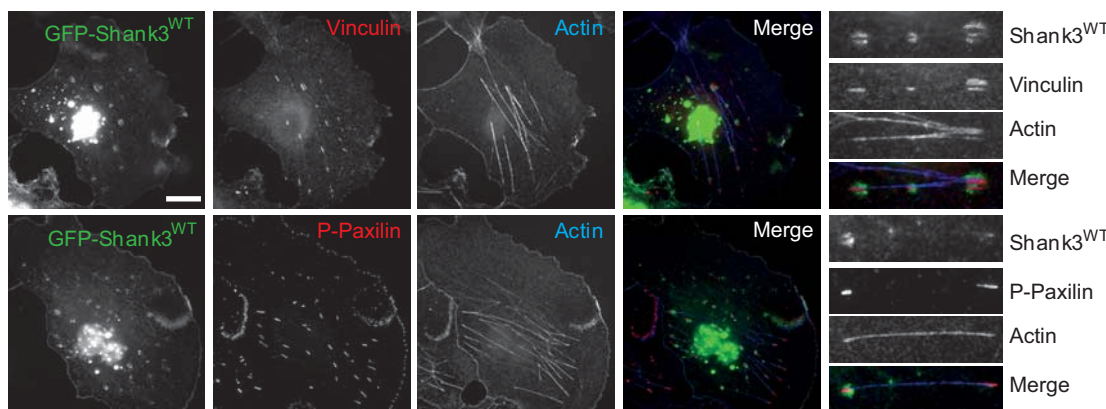
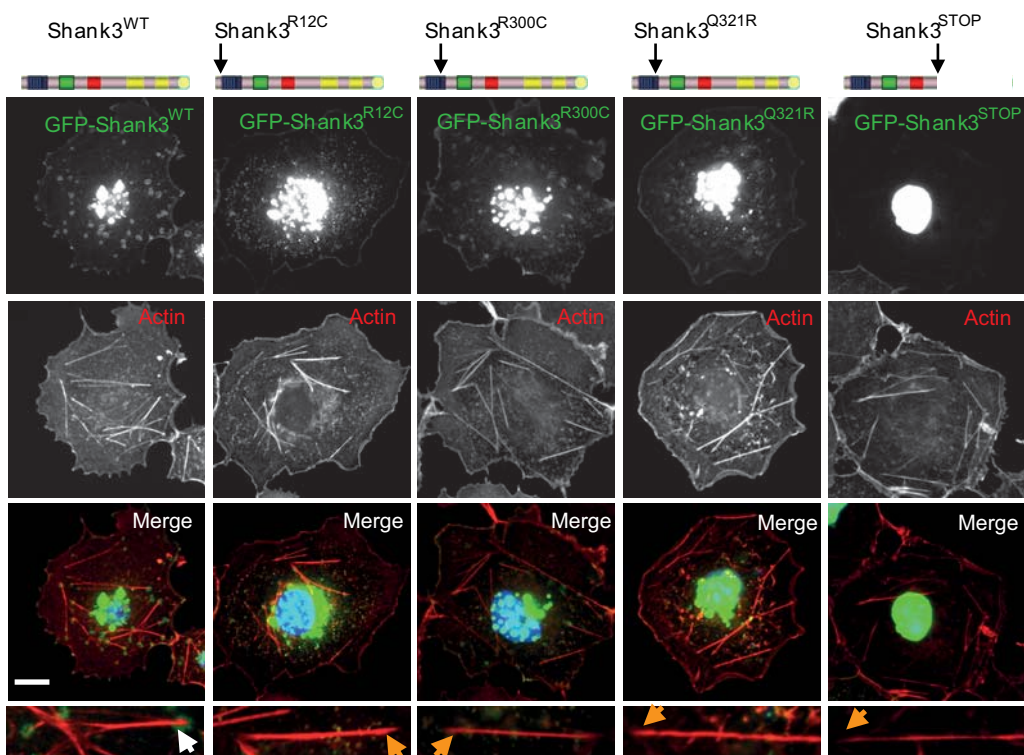
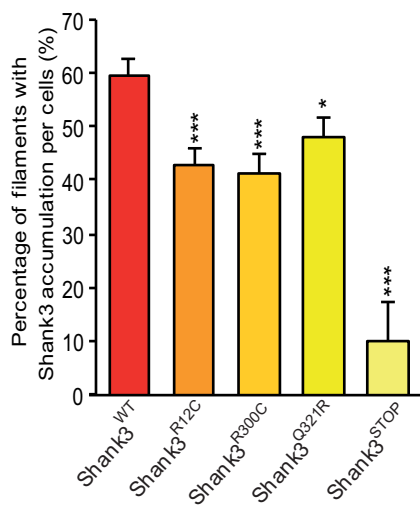
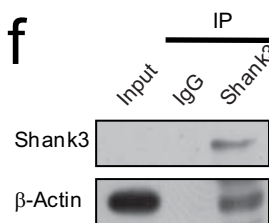
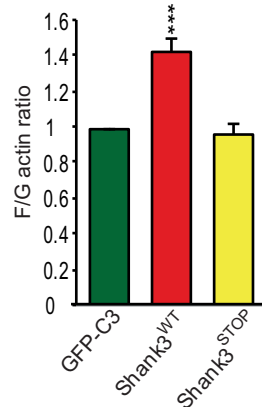
Figure 3: Effects of Shank3^{WT} and mutants on F-actin and cortactin levels in spines.

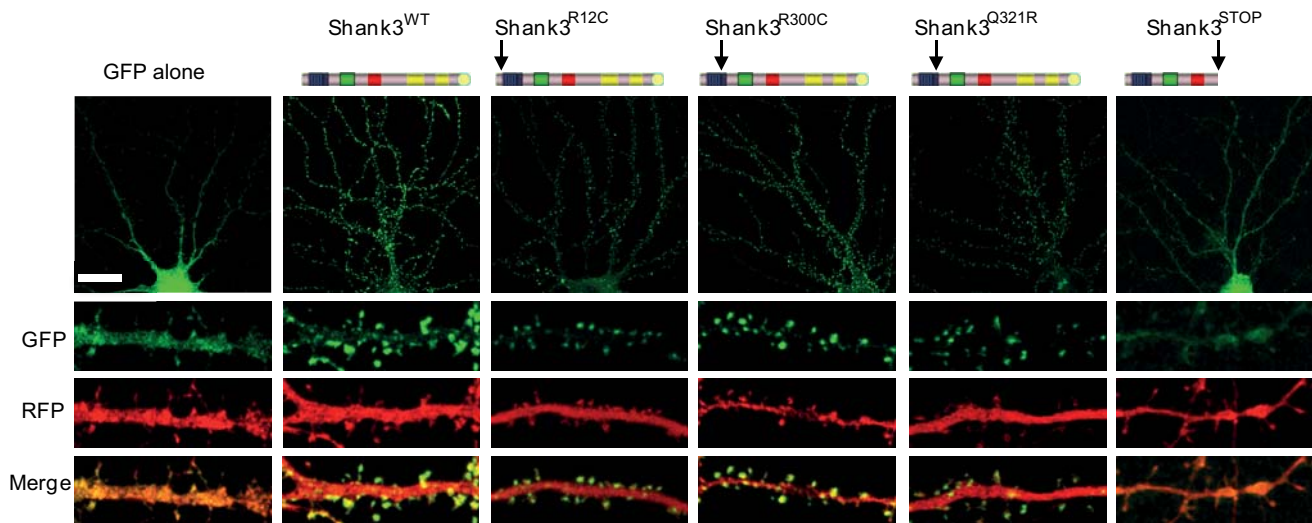
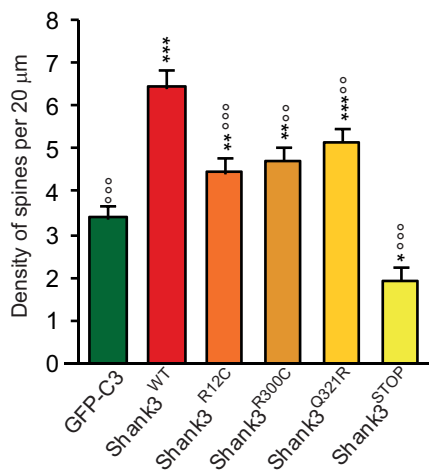
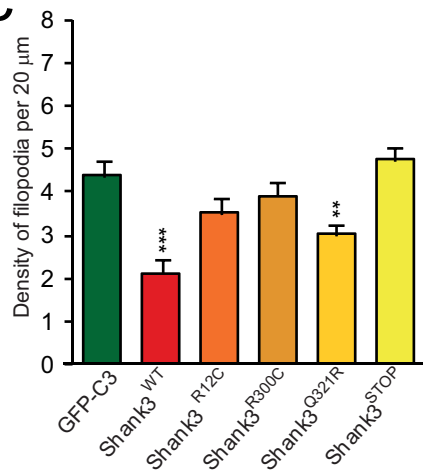
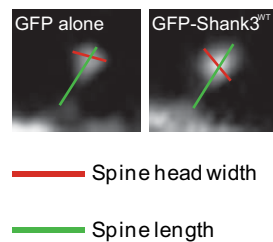
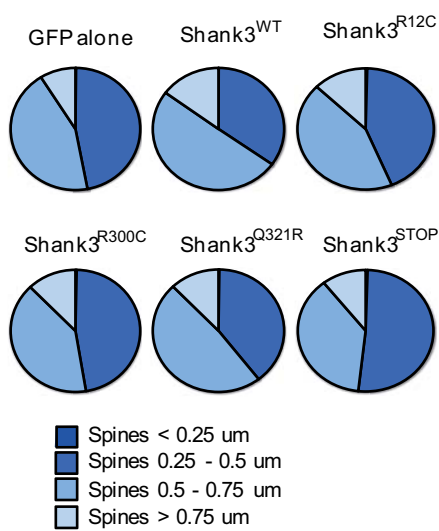
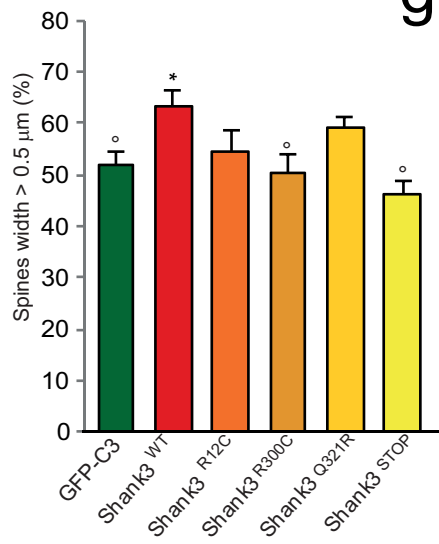
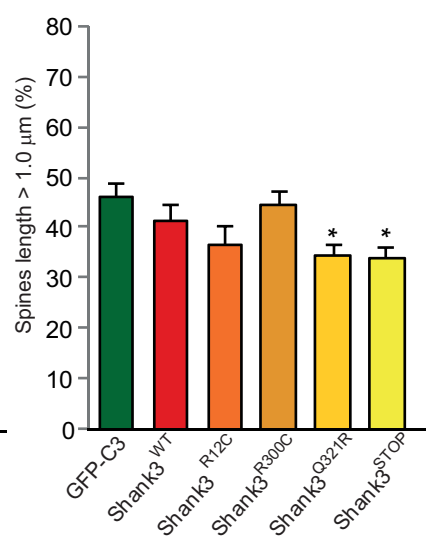
(a) Immunofluorescence microscopy of hippocampal neurons at DIV21 transiently co-transfected with GFP-Shank3^{WT} or mutated forms and RFP. Neurons are stained with anti-GFP and anti-DsRED. F-actin was visualized with phalloidin 647. Cortactin is visualized with anti-cortactin (blue). Scale bars represent 6 μ m. (b-c) Quantification of changes in the synaptic staining intensity of F-actin or cortactin induced by the overexpression of Shank3^{WT} or the mutated forms. (**p<0.01 compared with the control; °°p<0.001, °p<0.01, °p<0.05 compared with Shank3^{WT}).

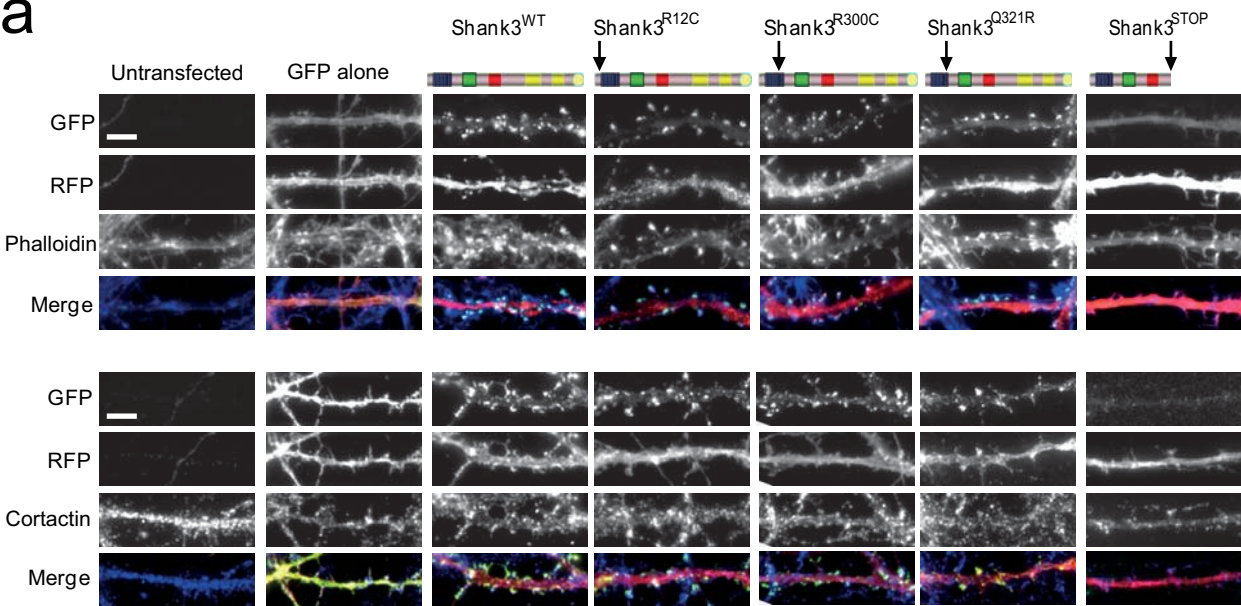
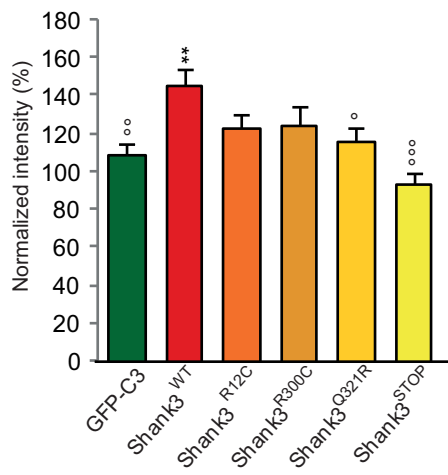
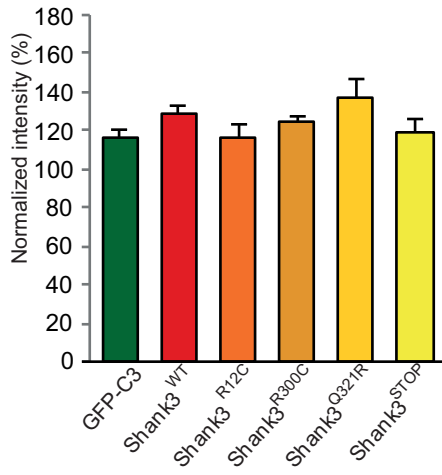
Figure 4: The Shank3 mutations decreased spontaneous neuronal activity. (a) mEPSCs recorded at -60 mV on hippocampal neurons (DIV21) transiently co-transfected with GFP-C3, GFP-Shank3^{WT} or mutated forms. (b) Quantification of mEPSCs frequency and amplitude under different transfection conditions. In Shank3^{WT}, there is a significant increase in mEPSC frequency. Each bar of the histogram is the mean \pm SEM of 10 experiments. ***p<0.001 and *p<0.05 compared with control; °°p<0.001, °p<0.01, °p<0.05 compared with Shank3^{WT}.

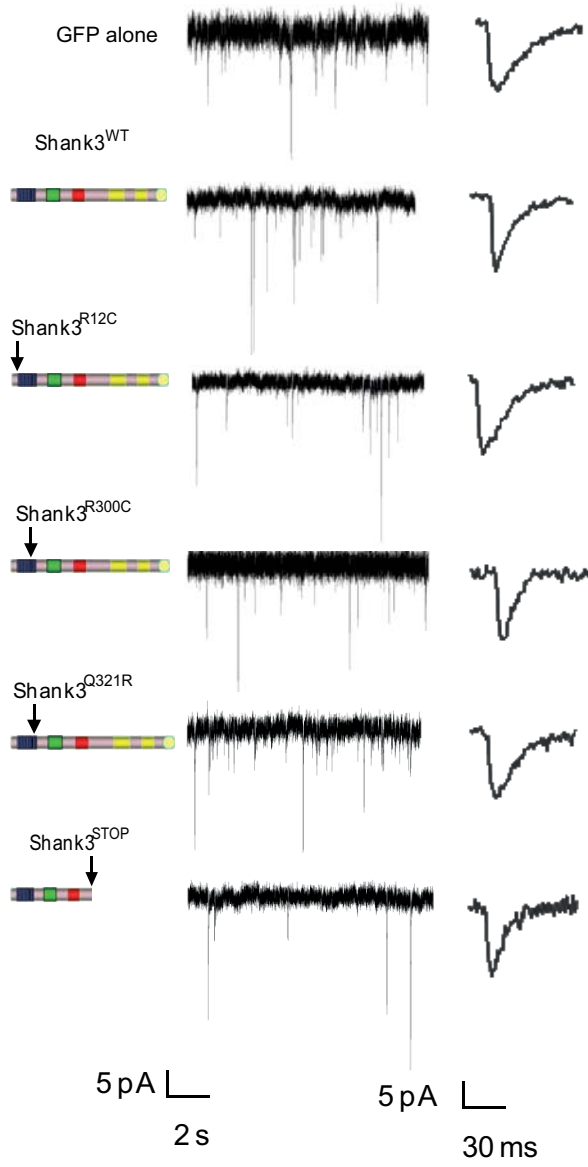
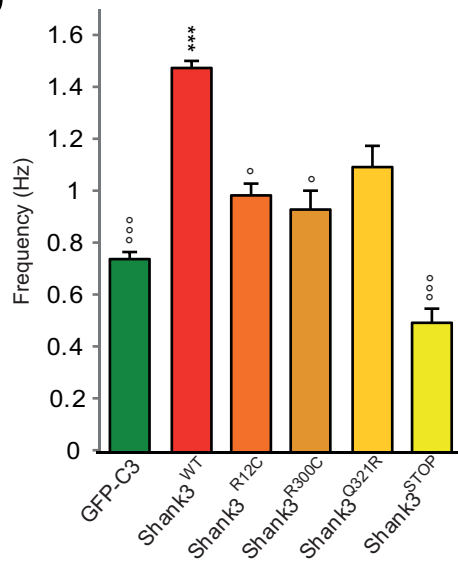
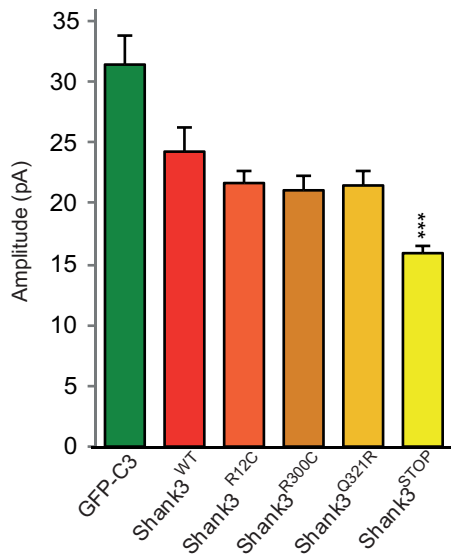
Figure 5: Effects of Shank3^{WT} and mutants on growth cone dynamics. (a) Shank3 is found in the growth cone of neonatal rat cultured hippocampal neurons on DIV2. Neurons are labeled for Shank3 (green), F-actin (phalloidin; blue), and either tubulin (anti-Tuj1; red) or cortactin (anti-cortactin, red). Scale bars represent 20 μ m. Insets represent high magnifications of the axonal growth cone. Shank3 co-localized with F-actin (blue) and with cortactin (red) in axonal growth cones. (b) Localization of Shank3 overexpressed in young neurons. GFP-Shank3^{WT} or Shank3^{STOP} or GFP-C3 (green) was transfected in young neurons (DIV0). Immunostaining for MAP2 (red) and actin (phalloidin; blue) revealed that Shank3^{WT} accumulates in growth cones, whereas Shank3^{STOP} is restricted to the cell body. (c) Time-lapse video microscopy of growth cones from rat hippocampal neurons co-transfected with the control (GFP-C3) and Shank3^{WT} or mutated forms. Merge represents three frames with different colors (0 min in green, 5 min in red and 10 min in blue). Scale bars represent 5 μ m. (d)

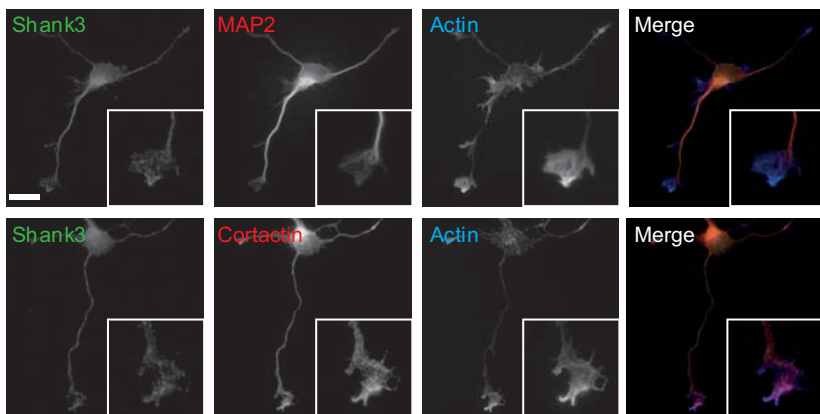
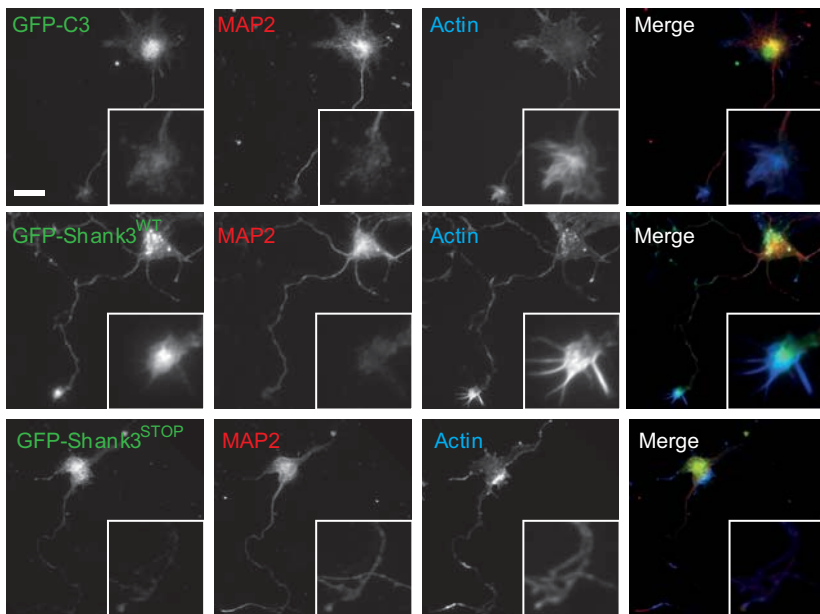
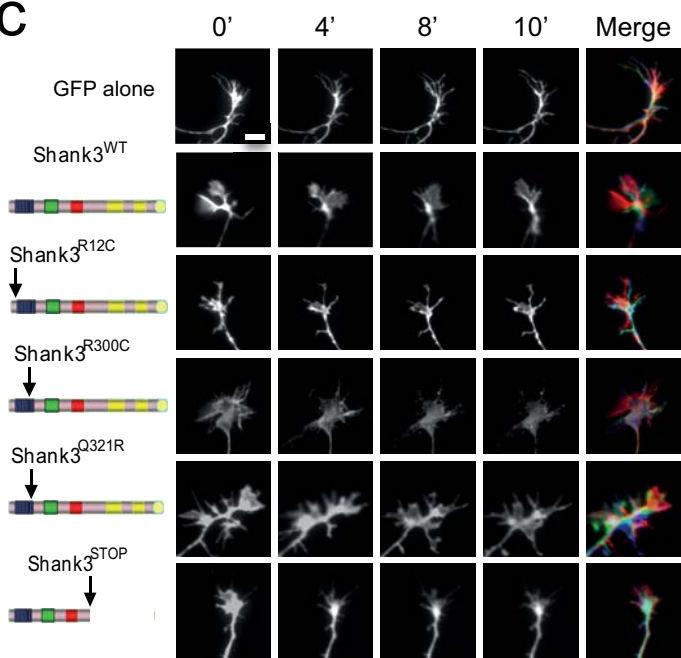
Quantification of growth cone motility with the motility index²⁸. ***p<0.001 and *p<0.05 compared with the control; °°°p<0.001 compared with Shank3^{WT}.

a**b****c****d****e****f****g****h**

a**b****c****d****e****f****g**

a**b****c**

a**b****c**

a**b****c****d**